5

Universal Growth Rate and Helical Reorganization in Self-organizing Knots

To this pattern decaying knots must adhere:
Pfirsh-Schlüter growth and unwind with no shear!
Unless pressure on axis entrained
Makes it kink out of the plane.
And sawteeth and islands and chaos appear!

In the previous chapters we have shown how a helical magnetic field can relax into a self-organized equilibrium. In this configuration the magnetic forces are balanced by a pressure force caused by a toroidal depression in the pressure, and equilibrium is attained when this low pressure region prevents further expansion into the higher-pressure external plasma. In this chapter we study the resistive evolution of these configurations generated from a new helical initial condition. Finite resistivity causes both a decrease in the magnetic field strength and a finite slip of the plasma fluid against the static equilibrium. This slip can be seen as Pfirsch-Schlüter diffusion, similar to what is seen in tokamak equilibria. The net effect is that the configuration, whilst constantly remaining in force equilibrium, slowly grows in size. The growth proceeds on a resistive timescale which is independent of the magnetic field strength and largely independent of the rotational transform. The rotational transform of the structure decreases according to a power law. At low magnetic field strength and high resistivity the initially axisymmetric magnetic configuration remains axisymmetric, and all field lines lie on nested toroidal magnetic surfaces. At higher field strength and lower resistivity a nonaxisymmetric perturbation occurs which introduces magnetic islands and magnetically chaotic regions in the structure. The appearance of these islands, and their time evolution is understood from the Hamiltonian dynamical system description of field line flow and the change in rotational transform.

5.1 Introduction

Spontaneous self-organization of magnetized plasma lies at the basis of many fascinating phenomena in both fusion reactor operation and astrophysical plasma observations. Novel approaches to fusion power generation rely on the generation of a self-organized MHD equilibrium [27,117]. Probably the most famous example of self-organization is the concept of Taylor relaxation [50], which states that a plasma self-organizes to a linear force free magnetic configuration with the same magnetic helicity as the initial field.

The Taylor hypothesis has been very successful in predicting the resultant configurations in toroidally confined plasmas, spheromaks and multipinches [118]. Recently there have however been reports on magnetic configurations that do not relax to a (linear) force free state, and do not exhibit Taylor relaxation. Yeates et al. have shown that there are additional topological constraints associated with the degree of field line mapping that prohibit the relaxation to a force free state in coronal loops. Also Moffatt has presented an example of one-dimensional relaxation that does not converge to the Taylor state [69]. In chapter 2 of this thesis we presented another example of relaxation to a self-organized equilibrium which is not force-free [70].

In chapter 2 we showed how linked rings of magnetic flux self-organize to a knotted magnetic structure where field lines lie on nested tori. The approximately axisymmetric field is in a Grad-Shafranov equilibrium [96], and the Lorentz force is balanced by a gradient in pressure force, caused by a lowering in pressure. The pressure is lowest on the magnetic axis, which is the degenerate torus at the center of all the nested toroidal magnetic surfaces. The magnetic topology of this structure is remarkable; the rotational transform is nearly constant from surface to surface, and as a consequence, the magnetic field line structure is topologically similar to the mathematical structure of the Hopf fibration [65] or its generalization to torus knots (chapter 2, [21]). In chapter 3 we used topology conserving relaxation on the Hopf fibration to show how the Hopf field relaxes to the Grad-Shafranov equilibrium. Using the virial theorem of MHD we showed that such an equilibrium, and not a Taylor state, is the only equilibrium that a localized field can attain.

Such localized states could occur in radio bubbles emitted from active galactic nuclei [26]. Also in earth-based plasma experiments localized fields are observed to conform to a toroidal shape in small-scale experiments [74] as well as the plasmoids ejected by e.g. a Marshall gun [75,76,77]. Also some models of magnetic clouds, magnetic structures observed in the solar wind that are correlated with plasma ejected from the sun by coronal mass ejections [78], assume a localized magnetic field carried by internal currents and balanced by the external plasma pressure [78,79,80,119,120].

One of the remarkable findings is how universally this structure is obtained from an initially helical field: it emerges from trefoils [70], twisted rings, and even Borromean

linked flux tubes [25]. In this chapter we study the emergence of this equilibrium starting from a new, highly linked initial condition. We study the time evolution of this structure as resistivity changes the magnetic topology and the magnetic field strength. The evolution of the structure is governed by two processes: First, the lowering of the magnetic field strength changes the equilibrium condition, such that the depression in pressure becomes lower. Second, finite resistance breaks the 'frozen in condition' of ideal MHD [83], allowing the plasma fluid to slip against the magnetic field lines of the configuration. The net effect is a fluid flow directed towards the region of lowest pressure. The combined effect of these two processes is a structure that grows on a resistive timescale.

The magnetic topology, characterized by the rotational transform of the magnetic surfaces, quickly reaches a nearly flat profile with a slight positive curvature. The rotational transform decays according to a power law, the characteristic exponent of which depends on the aspect ratio of the structure.

At low field strength and moderate resistivity the axisymmetry of the initial field is retained, and the decay follows a universal pattern. At high field strength and low resistivity the axisymmetry is remarkably broken, and the configuration becomes susceptible to a kinking of the magnetic axis. The resultant state bears a resemblance to the single helical axis (SHAx) state [121]. Surprisingly, the mode numbers of the kinking mode need not coincide with the mode numbers of any rational surface in the configuration. Continued reconnection after this axisymmetry is broken leads to the emergence of magnetic islands. A magnetic island is a region in the magnetic field where field lines do not form surfaces around the magnetic axis, but instead form toroidal surfaces, tubes that wind around the magnetic axis. The formation of magnetic islands is understood through the fact that magnetic field lines can be described by Hamilton's equations [122] and the breaking of axisymmetry perturbs the initially integrable Hamiltonian system.

The observation of these nonaxisymmetric equilibria in these self-organizing fields, and the destabilizing perturbations they lead to, can put limits on the regimes in which such structures can be found. A further understanding of these processes can shed light on the emergence of nonaxisymmetric equilibria in other contexts such as the SHAx state in reactors.

5.2 Initial field

As initial condition we use a highly helical initial state to generate the self-organizing magnetic structure. We construct an axisymmetric, helical initial field using cylindrical coordinates R, z, θ and flux functions $\psi_p(R, z)$ and $I(\psi_p)$. The coordinate system is shown in figure 5.1. Physically $\psi_p(R, z)$ represents the poloidal magnetic flux, passing through a circular surface of radius R around the z-axis (green circle). For $I(\psi_p)$ we choose a

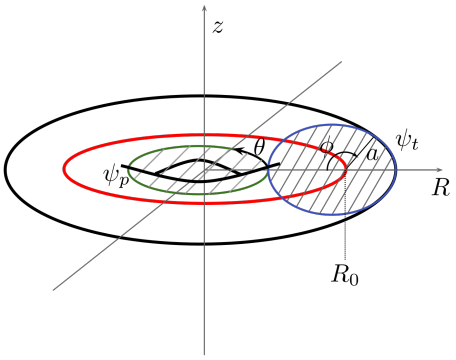

Figure 5.1: Coordinate system used for the construction of the initial magnetic field. The surfaces through which the toroidal flux ψ_t and poloidal flux ψ_p are defined are shown by the blue and green circles respectively. ϕ is the coordinate pointing in the poloidal direction of the torus, and θ is the coordinate pointing in the toroidal direction. The magnetic axis is given by the red circle located at $R_0 = 1$. The Hamiltonian dynamical systems description of a plasma discussed in section 5.6 also uses the coordinates defined here.

function that is constant on surfaces of constant ψ_p. I physically represents the total poloidal current, the current through the green shaded circle. The magnetic field is calculated from the flux functions by the standard methods for axisymmetric fields [63]:

$$B_R = -\frac{1}{R}\frac{\partial \psi_p}{\partial z}, \quad B_z = \frac{1}{R}\frac{\partial \psi_p}{\partial R}, \quad B_\theta = \frac{1}{R} I. \tag{5.1}$$

Using this construction guarantees that magnetic field is divergence free, and that field lines lie on magnetic surfaces of constant ψ_p.

We choose the following flux function:

$$\psi_p = \begin{cases} B_0 \cos^4\left(\frac{\pi}{2}\frac{a}{a_0}\right), & a \le a_0 \\ 0, & a > a_0 \end{cases}. \tag{5.2}$$

with B_0 a scaling parameter that sets the magnetic field strength and

$$a = \sqrt{(1-R)^2 + z^2}, \tag{5.3}$$

denoting the distance from the circle $R = 1, z = 0$, (indicated in red in figure 5.1) which is the magnetic axis of the structure. The magnetic axis consists of a single field line

around which other field lines wind. With this choice we can see that ψ_p is constant and zero for $a \geq a_0$ so that, according to equation (5.1), the poloidal field vanishes. The magnetic surfaces in the region where $a \leq a_0$ form concentric tori with circular cross section that enclose the magnetic axis.

We can choose any function for the toroidal current function I. For reasons that will become apparent in the next section we choose this function to be:

$$I = \frac{\psi_p \pi^2}{\iota_0 a_0^2}, \tag{5.4}$$

where ι_0 is a parameter that we can choose to vary the strength of the toroidal field. With this choice, also the toroidal magnetic field vanishes at $a \geq a_0$, and thus the field is an axisymmetric flux tube with major radius 1 and minor radius a_0 and $\boldsymbol{B} = 0$ outside of the tube.

5.2.1 Rotational transform profile

The winding of field lines in a toroidal magnetic structure is quantified by the rotational transform ι or its inverse, the safety factor q. The rotational transform geometrically represents the ratio of the number of times a field line wraps around the poloidal direction of a torus to the number of times it winds around the toroidal direction. The safety factor can be calculated using the well-known formula [123]:

$$q = \frac{1}{2\pi} \oint \frac{1}{R} \frac{B_\theta}{B_p} \mathrm{d}l, \tag{5.5}$$

where B_p is the magnitude of the poloidal magnetic field $B_R \hat{R} + B_z \hat{z}$, and the integration is carried out over a constant θ cross section of a magnetic surface $\psi_p = \text{const}$. This integration path is indicated by the blue circle in figure 5.1.

Because in the initial field the magnetic surfaces are concentric and symmetric around the magnetic axis, the term RB_p is constant on the surface. We choose to evaluate it at $z = 0, R \geq a$, where $\frac{\partial \psi_p}{\partial z} = 0$ and $\frac{\partial \psi_p}{\partial R} = \frac{\partial \psi_p}{\partial a}$.

$$RB_p = \frac{\partial \psi_p}{\partial a} = B_0 \frac{2\pi}{a_0} \cos^3\left(\frac{a\pi}{2a_0}\right) \sin\left(\frac{a\pi}{2a_0}\right). \tag{5.6}$$

The poloidal magnetic field is:

$$B_\theta = B_0 \frac{\pi^2 \cos^4\left(\frac{\pi a}{2a_0}\right)}{r \iota_0 a_0^2}. \tag{5.7}$$

On the magnetic surfaces the parameter a is a constant so the integral (5.5) becomes:

$$q(a) = \frac{\cos\left(\frac{a\pi}{2a_0}\right)}{4\iota_0 a_0 \sin\left(\frac{a\pi}{2a_0}\right)} \oint \frac{1}{r} \mathrm{d}l. \tag{5.8}$$

Using ϕ to parametrize the integral over the surface at a, and the identities $R = 1 + a\cos(\phi)$ and $\mathrm{d}l = a\mathrm{d}\phi$, we get:

$$\int_0^{2\pi} \frac{a}{1 + a\cos(\phi)} \mathrm{d}\phi = \frac{2\pi a}{\sqrt{1 - a^2}}. \tag{5.9}$$

This gives us the safety factor

$$q(a) = \frac{\frac{a\pi}{2a_0} \cot\left(\frac{a\pi}{2a_0}\right)}{\iota_0\sqrt{1 - a^2}}, \tag{5.10}$$

and hence a rotational transform of:

$$\iota(a) = \iota_0\sqrt{1 - a^2} \frac{\tan\left(\frac{a\pi}{2a_0}\right)}{\frac{a\pi}{2a_0}}. \tag{5.11}$$

The rotational transform profile is flat near the magnetic axis, and increases to infinity when $a \longrightarrow a_0$. At the magnetic axis the rotational transform is given by:

$$\lim_{a \longrightarrow 0} \iota(a) = \iota_0. \tag{5.12}$$

The initial condition is thus an axisymmetric, twisted magnetic flux tube lying in the x, y-plane. We can change the twist of the magnetic field lines by the parameter ι_0, and the toroidal magnetic field strength with the parameter B_0.

5.3 Time evolution

We simulate the time evolution of the helical magnetic fields numerically using the resistive, viscous, compressible isothermal MHD equations. The equations are solved using the PENCIL-CODE [32] on a numerical grid of 256^3 grid points in a cubic volume with side length of 5. See section 1.3 for the description of the code and the equations solved. The initial condition is calculated from equation (5.1) setting the parameter $a_0 = 4/5$ and varying the values of ι_0. The magnetic diffusivity η is varied and the kinematic viscosity ν is set to 2×10^{-4}. The simulation is run using open boundary conditions, by imposing a vertical component to the magnetic field on the boundary. In

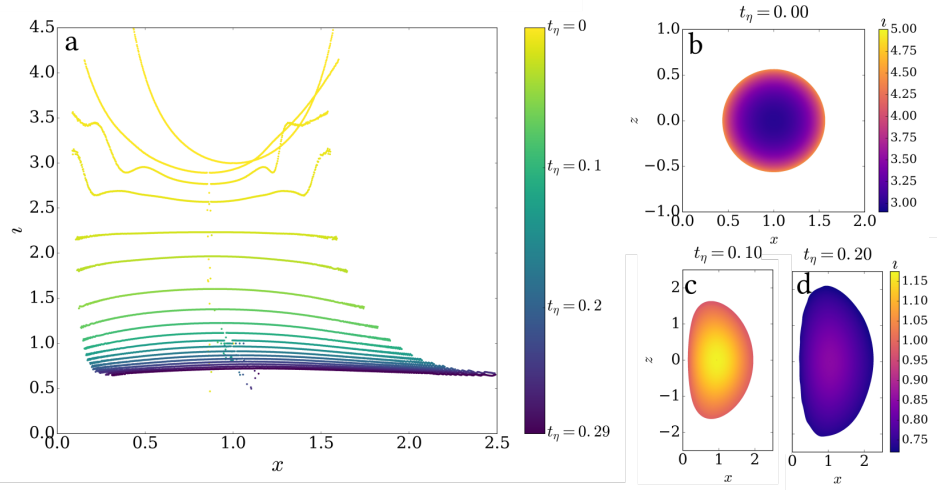

Figure 5.2: Creation of a self-organized equilibrium and change of rotational transform profile in time. Parameters for this run are: $\iota_0 = 3$, $B_0 = 0.05$ and $\eta = 2 \times 10^{-4}$. (a) rotational transform profile in time. (b) rotational transform profile in the initial field, corresponding to the top line in panel (a). (c) rotational transform plot at $t_\eta = 0.1$ and (d) rotational transform profile at $t_\eta = 0.2$. The rotational starts with strong positive curvature, but rapidly becomes nearly flat, with only a slight negative curvature.

this way magnetic field can escape from the simulation volume. The full field information is written out as a snapshot every 5 simulation time steps. The simulation is initialized with a constant pressure throughout the volume and the velocity field is zero. We scale the time to a resistive timescale using $t_\eta = tR_{\text{char}}^2/\eta$. For the characteristic length scale R_{char} we choose the distance of the magnetic axis from the origin in the initial field, $R_0 = 1$.

We analyze the resulting field configurations by using a field line tracing algorithm implemented in CUDA and running on graphics hardware. The hardware accelerated trilinear interpolation, and massive parallelization allows for a high speedup compared to CPU-based field line tracing. In the $(r, 0, z)$ plane field lines are traced from a 1024×1024 grid and for every field line the rotational transform is calculated.

The results of this analysis are seen in figure 5.2 (b) (c) and (d) for the field with ι_0=3, $B_0 = 0.05$ and $\eta = 2 \times 10^{-4}$. Every single pixel in these images is the result of analyzing the rotational transform of a single field line trace. In this run the magnetic field remains axisymmetric and the magnetic axis remains in the $z = 0$-plane. Figure 5.2 (a) shows the rotational transform profile at different times during the evolution of the configuration.

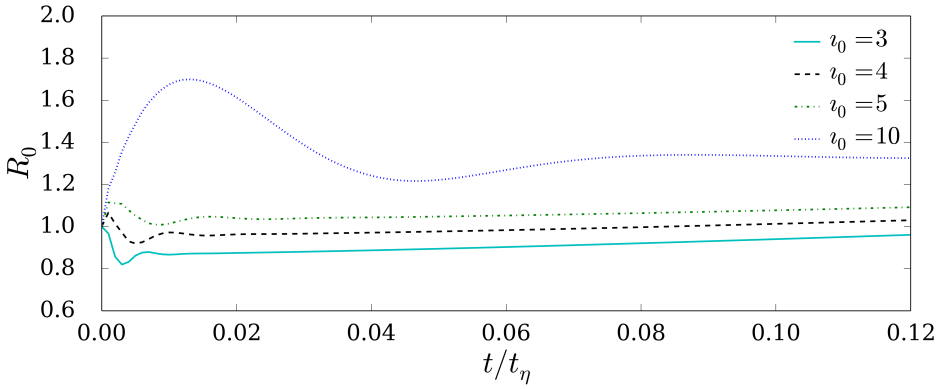

Figure 5.3: Position of the magnetic axis in time for different values of ι_0. The magnetic axis performs a damped oscillatory motion towards an equilibrium position which depends on the initial rotational transform, and then slowly grows. Except for ι_0 all parameters are identical with $B_0 = 0.05$ and $\eta = 2 \times 10^{-4}$.

The rotational transform profile quickly shifts from positively curved to nearly flat with a slight negative curvature, and subsequently slowly relaxes self-similarly. In the next sections we will study this decay by looking at the change in rotational transform and the shift in the location of the magnetic axis.

5.3.1 Resistive growth and decay of rotational transform

In figure 5.2 it is seen that the location of the magnetic axis first shifts inwards and then slowly expands. We follow these dynamics of the magnetic structure by extracting R_0, the distance from the origin to the magnetic axis. The magnetic axis is found in every simulation snapshot by an iterative fitting routine described in the appendix of chapter 1. This routine also finds the rotational transform of a surface at $R = 1.05R_0$. For continuity and speed of convergence we use the location of the magnetic axis of the preceding snapshot as the starting seed.

We track the position of the magnetic axis for several different values of ι_0 at constant $\eta = 4 \times 10^{-4}$. The results are shown in figure 5.3 for $\iota_0 = 3, 4, 5$ and 10. It is seen that the structure relaxes to an equilibrium radius, and then slowly increases in size.

We can understand this initial relaxation qualitatively from the interplay between magnetic tension and magnetic pressure described in section 1.2.3. Since the initial pressure is constant and the velocity is zero the initial motion of the fluid is purely due to

the Lorentz force $\boldsymbol{j} \times \boldsymbol{B}$. The field then evolves according to the following adage: magnetic rings contract and fatten, current rings expand and thin.

A high value of ι_0 results in a high poloidal field, and thus a stronger toroidal current, which will cause the initial ring to expand. The case of a low rotational transform will result in stronger toroidal field, and the structure will contract. In figure 5.3 we see that higher ι_0 leads to an initial expansion, and an equilibrium with a value of R_0 larger than 1, whereas low values of ι_0 lead to an initial contraction. The location of the magnetic axis performs a damped oscillation to the equilibrium position, and then slowly increases in size.

The later evolution of the structure proceeds on a purely resistive time scale. This is tested by simulating the evolution of the field with various values of resistivity. $\iota_0 = 3$, $B_0 = 0.05$ and $\eta = 2 \times 10^{-4}, 1 \times 10^{-4}$, and 5×10^{-5}. When rescaled to resistive time the growth of the structure and the change in rotational transform (of a surface at $R = 1.05R_0$) all collapse to a single curve indicating a universal growth mechanism, as shown in figure 5.4.

With the parameters used from above and $\iota_0 = 3$, the magnetic field strength B_0 doesn't affect the equilibrium reached or the rate of growth and change in rotational transform exhibited by these configurations. This is shown in figure 5.5, where the field with $B_0 = 0.05$ and $B_0 = 0.2$ are compared with $\iota_0 = 3$, $\eta = 2 \times 10^{-4}$. Despite a factor four difference in the magnetic field strength, the structures behave identically. It is nicely demonstrated in figure 5.5 that the initial relaxation to the equilibrium occurs on an Alfvénic timescale. The oscillation to the equilibrium R_0 lasts 4 times longer for the field where the magnetic amplitude is a quarter of the strength.

Whereas in a fusion device the magnetic topology is largely determined by outside control, and external coils can drive it to a certain regime, in these self-organizing structures all fields are caused by currents in the plasma that decay due to resistive losses. It is seen in all simulations that the rotational transform is monotonically decreasing in time. The rotational transform captures the ratio of toroidal winding to poloidal winding of the magnetic field lines on their respective magnetic surfaces, and can be calculated from equation (5.5). The observed lowering of rotational transform indicates that the poloidal magnetic field decreases at a faster rate than the toroidal magnetic field.

After an initial period where the structure organizes to the equilibrium configuration, the rotational transform decays according to a power law. The decay of the rotational transform is shown in figure 5.6. The characteristic exponent of this decay is different for runs with different ι_0. This affects the equilibrium radius of the structure, and thus the aspect ratio of the toroidal surfaces. A high value of ι_0 leads to an initial expansion in major radius, as is seen in figure 5.3. This will lead to a larger aspect ratio of the configuration, and from this we can conclude that structures with a larger aspect ratio exhibit a faster decay of the poloidal field compared to the toroidal field. The rotational

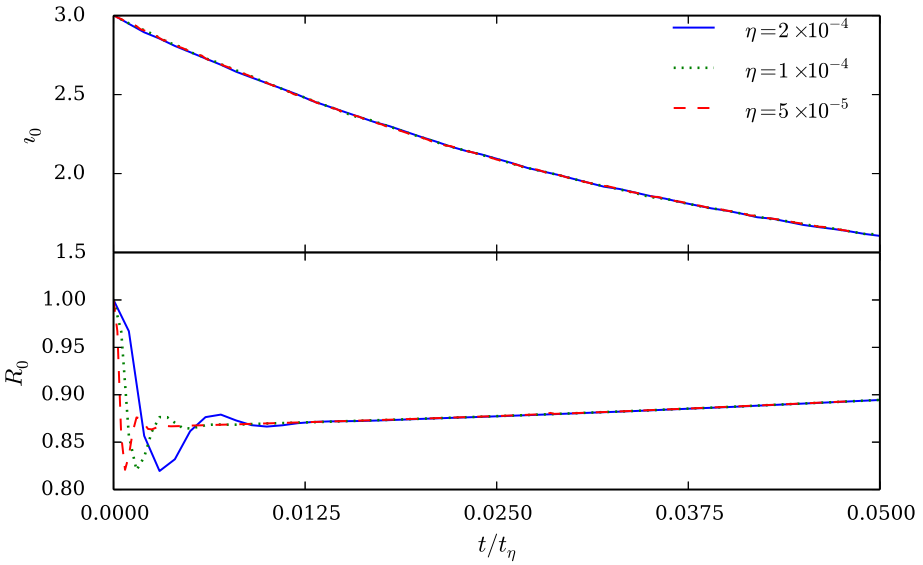

Figure 5.4: $\iota_0(t)$ and $R_0(t)$ vs resistive time for several different values of resistivity. The initial rotational transform is set to $\iota_0 = 3$, and magnetic field strength $B_0 = 0.05$. The change of the rotational transform and the radius of the structure all behave identically on a resistive time scale. The rotational transform was calculated from a surface at $R = 1.05R_0$.

transform between $t_\eta = 0.05$ and $t_\eta = 0.1$ is fitted with a power law $\iota_0(t) = at\eta^b$ and a characteristic exponent of 0.664 is found for the run with $\iota_0 = 10$ and 0.048 for the run with $\iota_0 = 3$. Guides are drawn in figure 5.6 showing $t_\eta^{-2/3}$ and $t_\eta^{-1/2}$ decay.

5.4 Pfirsch-Schlüter diffusion

In a perfectly conducting plasma, a magnetic field is effectively 'frozen in' and moves with the fluid motion [82,83,84], thus there can be no net flow of fluid perpendicular to the field lines. This would lead to a static MHD equilibrium such as those explored in chapter 3 of this thesis. When resistivity is included this restriction is lifted and the fluid can 'slip' against the static magnetic field lines. Field line slip is observed in many different scenarios and is one of the driving mechanisms behind $2D$ reconnection [124]. In the toroidal geometry of an operating tokamak, field line slip gives rise to slow diffusion out of the confinement region and is called Pfirsch-Schlüter diffusion [123].

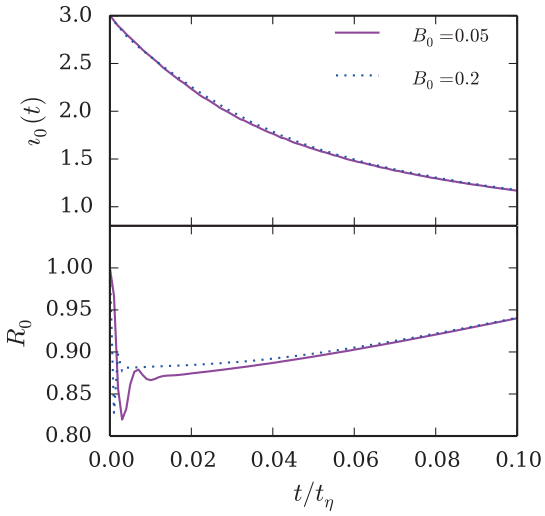

Figure 5.5: Magnetic decay of topologically identical structures with different magnetic field strength B_0. Despite the difference in magnetic field strength The change in rotational transform proceeds at exactly the same rate, and the equilibrium radius is identical. Note that the initial oscillations towards the equilibrium radius occur on the Alfvénic timescale: the oscillations to the equilibrium configuration proceed at a four times faster rate when $B_0 = 0.2$ then when $B_0 = 0.05$.

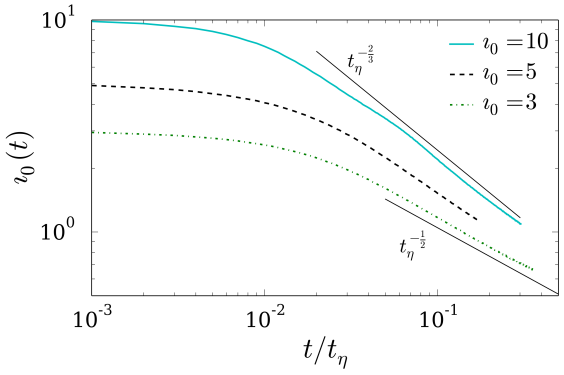

Figure 5.6: Time dependence of the rotational transform for different values of ι_0. After the initial period where the magnetic structure re-organizes on an Alfvénic timescale, the rotational transform decays following a power law with characteristic exponent between −2/3 and −1/2. The rotational transform was calculated for a surface close to the magnetic axis, located at $R = 1.05R_0$.

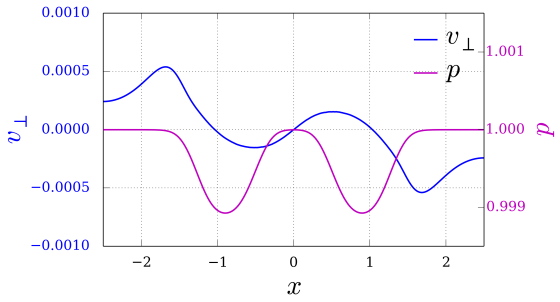

Figure 5.7: Fluid velocity and pressure profile along the x-axis. The magnetic axis is located at the minimum in pressure. The flow profile shows a net influx of plasma towards the magnetic axis.

This Pfirsch-Schlüter flow is directed outwards, in the direction of the pressure gradient.

In the self-organized structures considered here a similar magnetic slip causes a diffusion of plasma fluid into the magnetic structure. This is shown in figure 5.7, where the flow field is plotted along the x-axis together with the pressure profile. The magnetic axis is located at the minimum of the pressure, and it is clearly seen how there is net fluid flow directed towards the magnetic axis. The slight discrepancy between the location of the magnetic axis and the zero of the velocity is due to the axis itself being in motion.

Whilst the fluid flow slowly penetrates the magnetic structure, the magnetic energy in the structure is decreasing. The decrease of total magnetic energy for the simulations with $\iota_0 = 3$ and $B_0 = 0.05$ is shown in figure 5.8. Note that the magnetic field strength decays at a much faster rate than the resistive decay time t_η.

5.4.1 Relation to magnetic clouds

It is important to note that the decay in rotational transform is fast compared to the increase of the major radius of the structure; the rotational transform changes by a factor of three in the time R_0 only changes a few percent. This is important when considering this equilibrium as a model for magnetic clouds.

A magnetic cloud is a localized magnetic structure in the interplanetary plasma with increased magnetic field strength observed by passing satellite probes, and correlated with coronal mass ejections [78]. The magnetic field direction varies over a large angle during the passage, but due to the low density of probes in the interplanetary medium, a measurement of the full magnetic structure is impossible. There are several models for magnetic clouds discussed in literature, see for example [78] for an overview. One of the more common models is of a magnetic cloud as a long flux rope extending, and still

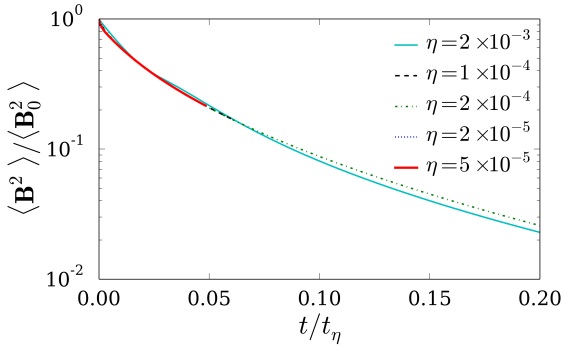

Figure 5.8: Decay of magnetic energy vs time for the runs with $\iota_0 = 3$ and $B_0 = 0.05$ for different values of resistivity.

magnetically connected to the surface of the sun. Nevertheless there are several models that consider magnetic clouds as localized magnetic excitations, carried by internal currents.

Kumar and Rust describe a model for a magnetic cloud as an isolated, net current carrying toroidal flux ring [79]. The magnetic field inside the ring is based on the force-free Lundquist solution valid for an infinite cylinder [125]. As they themselves note, this cannot be an exact description, as the toroidal geometry necessitates the existence of a hoop force such as described in [120]. In this model the plasma current is zero outside of the toroid, but the net current is non-zero such that the ring generates its own force-free field.

There are several differences between Kumar and Rust's model and a magnetic cloud as a self-organized structure we describe. Firstly the magnetic field in their model is based on force-free solutions. We have shown in chapter 3 that a localized magnetic field can never be in equilibrium without a dip in pressure, and a balance between the Lorentz force and the pressure force. The rotational transform profile in their model is also very different. In Lundquist solutions the axial and tangential fields (which, when the cylinder is translated to a torus, correspond to the toroidal and poloidal directions respectively) are given by Bessel functions. As such the rotational transform profile changes significantly from the magnetic axis to the edge [126]. The magnetic field outside the ring is purely toroidal, which implies that the rotational transform goes to infinity. Even though their model resembles the configuration we describe superficially, the rotational transform profile is drastically different, and our simulations show that the profile quickly becomes nearly flat.

Another magnetic cloud model which resembles the configurations we observe is the

flare-generated spheromak model by Ivanov and Harshiladze [80] and further explored by Vandas et al. [119]. They describe the clouds using the spherical force-free solution of Chandrasekhar and Kendall [127]. The magnetic topology in this solution also consists of field lines lying on nested toroidal surfaces. The rotational transform profile in these force-free solutions is not constant either.

The resistive decay time $t_\eta = \mu_0 R_{\text{char}}^2/\eta$ for a structure with $R_{\text{char}} = 10^6$km is 1.7×10^9 years [62], so on that timescale change in the rotational transform profile is expected to be small. The reconnection process leading to the formation of the self-organized localized equilibrium however takes place on a much faster, Alfvénic timescale. The evolution of the magnetic structure, after it is generated, can therefore be considered to be approximately ideal, as is also assumed in the model by Ivanov and Harshiladze and the model by Kumar and Rust.

Because the structure we describe does not rely on the assumption of force free fields, we speculate that the magnetic structures described in this thesis are a more realistic model for localized magnetic clouds than the two others described above. Our model predicts a fundamentally different rotational transform profile from the other models discussed above, and more research is needed to determine which model best describes the observations.

5.5 Nonaxisymmetric perturbations

The resistive evolution of the self-organizing structure is a robust phenomenon that happens self-similarly for different values of resistivity, rotational transform, and magnetic field strength. In the simulations presented above, the field remains axisymmetric during the entire evolution, and the entire structure consists of nested toroidal magnetic surfaces. When the resistivity is set below 5×10^{-5} however, this pattern is broken.

Figure 5.9 shows $\iota_0(t)$ an $R_0(t)$ for the run with $\eta = 2\times10^{-5}$ and $\eta = 2\times10^{-4}$. The initial rotational transform $\iota_0(0)$ was set to 3 and B_0 is 0.05 for both runs. The lower resistance run is seen to deviate from the above-described pattern: The rotational transform remains at exactly 2 for a period, and the radius of the magnetic axis increases starting from $t_0 = 0.01$. In the interval between $t_\eta = 0.025$ and $t_\eta = 0.03$ R_0 sharply increases and then decreases.

In order to understand this behavior we look at the magnetic structure as a function of time by drawing a Poincaré plot at several times during this interval in figure 5.10. At $t = 0.023t_\eta$ the position of the magnetic axis has shifted from the geometrical center of the magnetic surfaces. At $t = 0.0266t_\eta$ a new region is seen to emerge, where magnetic field lines form toroidal surfaces that do not enclose the magnetic axis. The new region emerges from a surface where the rotational transform is 2. Such a region is called a

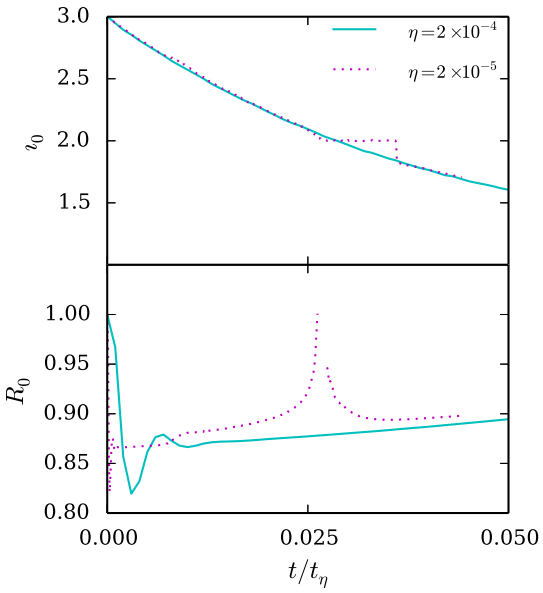

Figure 5.9: The rotational transform and radius versus resistive time for the fields with parameters $B_0 = 0.05$, $\iota_0 = 3$, and different values of resistivity of $\eta = 2 \times 10^{-4}$ and $\eta = 2 \times 10^{-5}$. The deviation of the low-resistance run is caused by a nonaxisymmetric perturbation appearing.

magnetic island, and the processes leading to the formation of magnetic islands will be discussed in section 5.6.

Eventually the new region replaces the original magnetic axis, which shrinks and disappears. This process is similar to the marginal core interchange mechanism proposed as an explanation for the sawtooth oscillations seen in tokamaks [128].

Sawteeth are observed when a tokamak is driven to a state where $\iota \geq 1$ near the magnetic axis. A (1,1) island is formed on the resonant $\iota = 1$ surface that grows until it replaces the magnetic axis. In a reactor the magnetic configuration is driven by currents in the external coils, and kept quasi-static such that this mechanism is continuously repeated. This leads to a slow buildup of temperature on the magnetic axis which is quickly depleted during a fast reconnection event that replaces the plasma on the magnetic axis with the colder plasma from the resonant surface. This process repeats periodically, leading to a characteristic sawtooth pattern in the electron temperature. A quiescent regime can also occur where the mechanism is saturated due to a helical flow field in the central region [129].

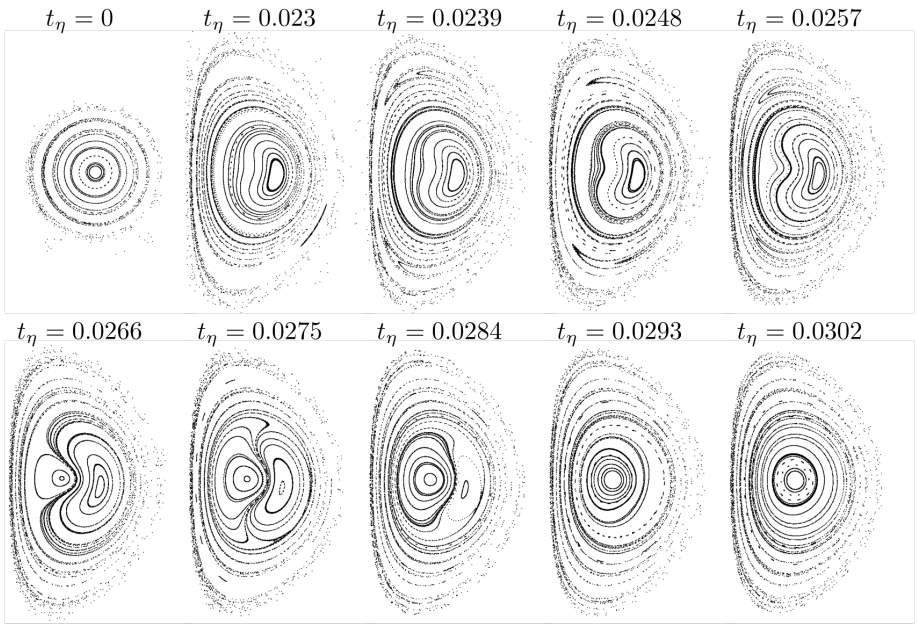

Figure 5.10: magnetic structure during the core interchange process. Run parameters are $B_0 = 0.05$, $\iota_0 = 3$, and $\eta = 2 \times 10^{-5}$. The island that replaces the core of the structure originates from the surface with $\iota = 2$.

Whereas in an inductively driven tokamak the magnetic configuration is kept quasi-static due to the constant drive, these self-organizing and expanding magnetic equilibria are continuously lowering in rotational transform. This causes the core interchange to be a one-off event that only occurs when a resonant magnetic surface with $\iota \in \mathbb{N}$ approaches the kinked magnetic axis. We will now describe the three dimensional structure of the magnetic surfaces during this process.

5.5.1 Kinked configuration

Just before the core interchange takes place the magnetic axis is seen to be located away from the geometrical center of the magnetic surfaces. A Poincaré plot and a select magnetic surface are shown in figure 5.11 at $t_\eta = 0.025$. The magnetic surface shown in blue in the Poincaré plot has become kinked, and so has the magnetic axis in the structure. The kinking of a surface near the magnetic axis is shown in figure 5.11 (b) and

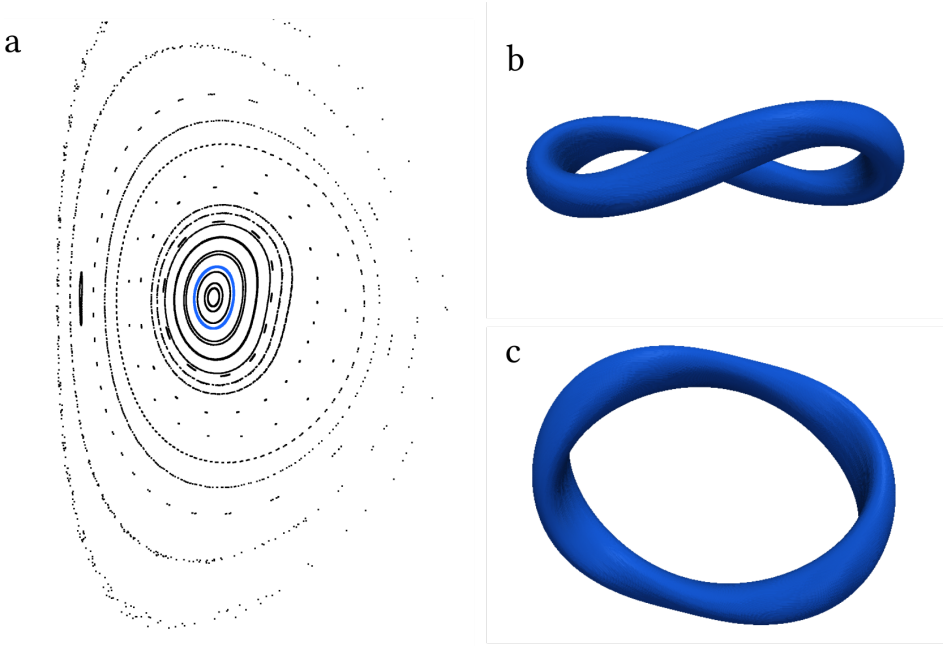

Figure 5.11: Magnetic structure in a perturbed configuration taken at time $t = 0.025t_\eta$, $\eta = 2 \times 10^{-5}$ $\iota_0 = 3$. (a) Poincaré plot. The magnetic surfaces are deformed in the region around the magnetic axis. A magnetic surface close to the magnetic axis is shown in blue. (b) Side view of the magnetic surface close to the magnetic axis. (c) Top view of the magnetic surface near the magnetic axis. This magnetic surface, and those around it, are kinked.

(c), and is clearly 2-fold symmetric around the z-axis.

The deformation of the magnetic axis in the structure is the reason that the computed value of R_0 in figure 5.9 increases. The kinking of the axis results in a larger distance between the origin and the point on the magnetic axis that is found by the fitting routine, resulting in an overestimation of the radius. With this we can also understand the deviation exhibited in the rotational transform. Because the kinking of the axis causes the estimation of poloidal and toroidal winding numbers to be equal to the mode numbers of the kink, the calculation of the rotational transform results in a constant value of 2.

This kinked configuration is already present at $t_\eta = 0.01$ and remains at a stable amplitude until $t_\eta = 0.025$. In this configuration the magnetic surfaces form a continuous foliation of nested tori around the magnetic axis that can be seen as a deformation of the initial magnetic surfaces.

We hypothesize that the driving mechanism behind this nonaxisymmetric deformation is caused by the influx of plasma to the magnetic axis through Pfirsch-Schlüter diffusion. This results in a higher pressure on axis than the global equilibrium can maintain. The helical deformation of the magnetic axis effectively increases the length of magnetic surfaces, but not the cross-sectional area. Since fluid pressure is constant on magnetic surfaces, this deformation allows the same pressure on axis to be maintained. This inflow hypothesis is supported by the observation that this nonaxisymmetric deformation is stronger, and occurs faster at higher magnetic field strengths, when the dip in pressure and the resultant diffusion are larger. Configurations with stronger magnetic field strength will be discussed below in section 5.7.

Helically perturbed magnetic equilibria have been the subject of much recent investigation. Notably, Lorenzini et al. described a helical equilibrium in the RFX-mod field-reversed-pinch (FRP) device [121]. In an FRP, although the plasma vessel is topologically identical to that of a tokamak, the rotational transform is generally much higher. A larger proportion of the magnetic field is generated by the internal plasma currents, and the resultant equilibria are generally much more unstable. In the RFX-mod experiment at a high currents (above 1 MA) the magnetic configuration is seen to self-organize into helical configurations in a regime dubbed the Quasi-Single Helicity (QSH) regime [130,131]. In this regime the magnetic axis forms a kinked, spiral curve that is surrounded by a significant region of closed magnetic surfaces with good confinement properties. This state is dubbed the Single Helical Axis (SHAx) state. Due to the in general high amount of chaos present in the FRP configuration, the SHAx state is surrounded by a significant chaotic plasma region.

In [121] the FRP was operated in the regime where the rotational transform at the center is predicted to be $\iota_0 = 7$, and the axis is kinked such that it makes exactly 7 rotations around the geometrical axis of the device. The magnetic configuration in this kinked equilibrium is also reproduced by ideal equilibrium codes [132,133], even at zero pressure, when the correct initial flux functions are prescribed. These can be generated from the axisymmetric toroidal equilibrium solution plus the toroidal and poloidal fluxes of the dominant mode [121].

Our results show that a helical deformation of the magnetic axis can also occur in our MHD equilibrium setting and with a different mechanism causing the helical deformation. It is also notable that this nonaxisymmetric reconfiguration occurs at a moment when the rotational transform is nowhere resonant with the perturbation. In Figure 5.9 it is seen that the perturbation starts when $\iota_0(t) = 2.5$. These results demonstrate a new mechanism for driving nonaxisymmetric perturbations in MHD equilibria in which the effect of plasma pressure is essential. Since the improved confinement of plasma around the magnetic axis in the SHAx state observed in FRPs leads to localized heating, and thus an increase in pressure around the axis, it is possible that such mechanisms also

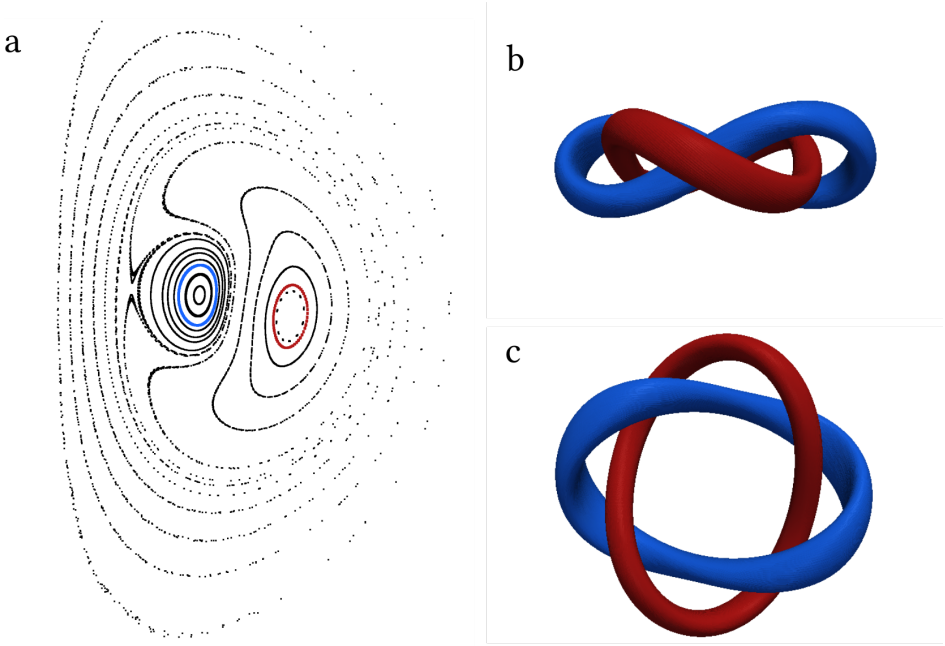

Figure 5.12: Magnetic structure in a nonaxisymmetrically perturbed configuration at $t = .028t_\eta$. (a) Poincaré plot. The configuration exhibits a double helical axis state, with two helical magnetic axes. (b) Side view of two magnetic surfaces close to the two magnetic axes. (c) Top view of the two magnetic surfaces.

play a role in their formation.

5.5.2 Core exchange and return to axisymmetry

This stable, kinked configuration is maintained right up to the point that the rotational transform approaches the value 2.0. At that point a magnetic island is formed on the surface with $\iota = 2$, and a double axis (DAx) [134] state is achieved. A Poincaré plot and two surfaces around the two magnetic axes are shown in figure 5.12.

Since the rotational transform profile is continuously changing, the location of the resonant surface continuously changes in time. The size of the island grows in time, and the region of magnetic surfaces enclosing the magnetic axis shrinks until the original axis disappears, and the field line at the center of the island forms the new magnetic axis.

After the core interchange process has completed, the configuration becomes ax-

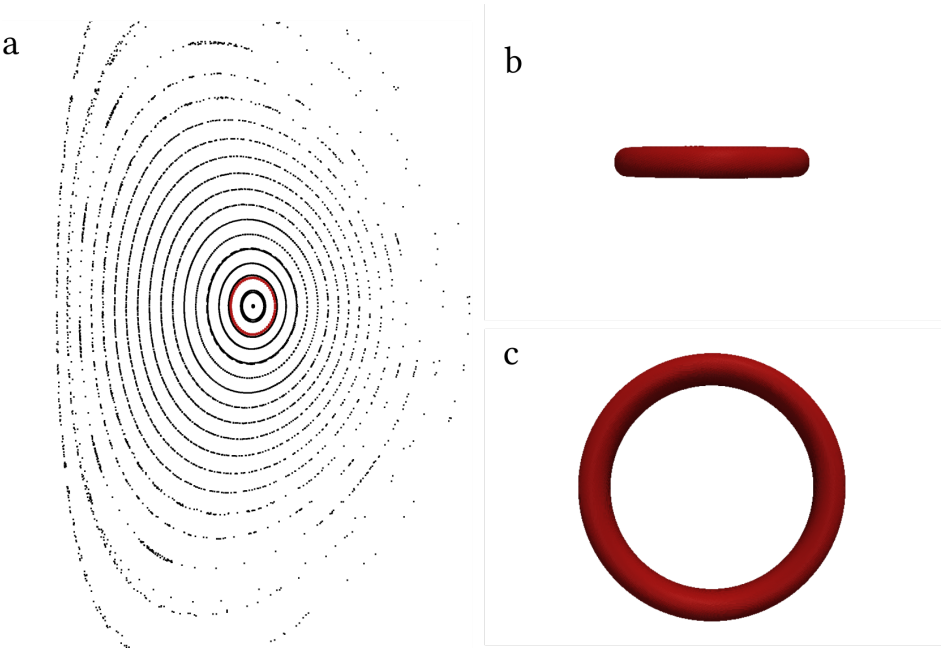

Figure 5.13: Magnetic structure after the nonaxisymmetric perturbation has resulted in a core interchange mechanism, and the field has returned to an axisymmetric equilibrium at $t = 0.04t_\eta$. (a) Poincaré plot. (b) Side view of the magnetic surface close to the magnetic axis. (c) Top view of the magnetic surface near the magnetic axis.

isymmetric. The state has a single magnetic axis and all magnetic surfaces lie around this axis. A Poincaré plot of the axisymmetric configuration is shown in figure 5.13.

5.6 Magnetic islands

Magnetic islands are a well known phenomenon in fusion reactors such as Tokamaks. They are magnetic structures that disrupt the neat organization of nested toroidal magnetic surfaces. These structures occur when perturbations break apart rational magnetic surfaces (surfaces where the rotational transform ι is a rational number). Only one closed field line of the former rational surface remains and forms an (n, m) torus knot. Other nearby field lines form a magnetic surface around this close field line. Investigation of the magnetic island structure has recently successfully been used to calculate the topology of the Wendelstein 7-X stellarator magnetic field to unprecedented precision [135].

It was only discovered fairly recently that this phenomenon can be understood by the mathematical correspondence between the equations governing field line flow and the equations governing $1\frac{1}{2}$ degree of freedom Hamiltonian dynamical systems [122,136,137]. In Hamiltonian dynamical systems the time evolution of the canonical variables p and q are governed by a Hamiltonian $H(p, q, t)$ that obeys Hamilton's equations:

$$\frac{\partial p}{\partial t} = -\frac{\partial H}{\partial q}, \quad \frac{\partial q}{\partial t} = \frac{\partial H}{\partial p}. \tag{5.13}$$

The description of a magnetic field can (under certain conditions) be cast in exactly the same mathematical structure. Even though mathematically equivalent, the effective Hamiltonian $H(p, q, t)$, the canonical variables p and q and the interpretation of the 'time' t are not obvious. The Hamiltonian is given by the poloidal magnetic flux ψ_p, as defined in figure 5.1. The canonical variables p, q, and t are respectively ψ_t, the toroidal magnetic flux, ϕ, the poloidal angle, and θ, the toroidal angle. See [122] for a recent review of nonaxisymmetric fields and a derivation of the magnetic field line Hamiltonian, or [138] for a mathematically very accessible treatment of this subject. It is important to stress that the variable which takes the place of time is θ, a coordinate in actual space, and that this formalism describes the magnetic field only at one instance of its evolution in time.

The canonical coordinates used in the Hamiltonian are constructed from the magnetic field itself. Figure 5.1 shows the coordinate system used for the construction of the initial field, and the canonical coordinates that correspond to it. Also for different, even nonaxisymmetric fields that consist of nested toroidal magnetic surfaces, a coordinate system like this can be constructed. Such a field, in reference to the dynamical systems notion of integrability, is referred to as an integrable field. The power of this formalism is not to accurately describe fields consisting of nested toroidal magnetic surfaces, but to understand the fields that we observe in plasma and simulation as the result of such an integrable field and additional perturbations. The study of perturbations to Hamiltonian dynamical systems is a rich and broad research area, whose results can now be applied to understand the variety of magnetic structures observed. It is well known for example that adding a perturbation to an integrable Hamiltonian dynamical system leads to period doubling, as in the driven harmonic oscillator.

In the magnetic field line Hamiltonian we can look at a perturbation of ψ_p in a field with perfect magnetic surfaces:

$$\tilde{\psi}_p = \psi_p + \epsilon \cos(n\phi + m\theta), \tag{5.14}$$

where ϵ is a small parameter. Since ϕ and θ are spatial coordinates, this corresponds to adding a spatially-varying poloidal flux to the configuration. This deforms the original magnetic surfaces, but more significantly, if a magnetic surface with $\iota = n/m$ is present

in the configuration, this surface breaks up into a magnetic island. If several resonant surfaces exist, or if the perturbative term contains more components than just the one described above, several magnetic surfaces will be broken up into island chains. The intermediate surfaces will be deformed by the presence of magnetic islands, and form secondary island chains. When the perturbations are large enough these islands will overlap and a fully chaotic region will develop in accordance with the Chirikov overlap criterion [139,140]. The Hamiltonian description for fields derived from the Hopf map (equation (3.3)) has been described by Joost Opschoor, as well as investigating perturbations of the above form [138].

With this we can understand the evolution of the configurations which exhibit the nonaxisymmetric perturbation as for example seen in figure 5.9 and 5.11-5.13. Initially, the magnetic field is axisymmetric, but the increase of pressure on the magnetic axis causes it to kink. In this nonaxisymmetric configuration, the change in magnetic field due to resistivity is no longer distributed evenly as a function of θ, such that the poloidal flux function ψ_p gains perturbative terms. At $t_\eta = 0.025$ there are no resonant surfaces present, so this only causes a deformation of the intact non-resonant surfaces.

The rotational transform in the entire structure continuously lowers and at $t_\eta = 0.028$, the surface with rotational transform $\iota = 2$ is present in the configuration. The nonaxisymmetric flux induced by resistive processes during the kinked configuration is resonant with this surface, and a magnetic island is formed as is shown in figure 5.12. As the field evolves, the rotational transform continues to lower. Because the rotational transform profile is positively curved, the location of the perturbed resonant surface comes closer to the magnetic axis.

At a certain point it becomes equivalent to describe the new island as a perturbation of the original structure or the original magnetic axis as a perturbation to the configuration with the new magnetic axis. As the rotational transform continues to lower, the resonant surface disappears from the configuration, and the original axis is replaced. As the rotational transform in the entire structure is now below 2, there are no more resonant surfaces.

At this point the magnetic field strength has lowered to a point where the structure is no longer susceptible to kinking of the magnetic axis. As the field evolves further, resistivity continues to decrease the magnetic field strength. Since the effects of resistivity are stronger when the spatial gradients of the magnetic field are higher, the perturbation, which has larger spatial gradients than the integrable field, will decay faster than the global axisymmetric field. Therefore the field returns to an axisymmetric configuration as is seen in figure 5.13.

5.7 Higher field strength: onset of chaos

When the magnetic field strength is higher, the dip in pressure on the magnetic axis required for the equilibrium becomes larger, and so do the diffusion processes leading to kinking of the magnetic axis. This is seen in the evolution of a field with parameters $\iota_0 = 5$, $\eta = 2 \times 10^{-4}$, and $B_0 = 0.2$. The magnetic axis becomes kinked and distorted almost immediately, and the field around the magnetic axis becomes chaotic. Note that the field with $B_0 = 0.2$ and $\iota_0 = 3$ and otherwise identical parameters shown in figure 5.5 remained axisymmetric and did not exhibit magnetic chaos.

When the rotational transform reaches a value of three, a double magnetic axis state appears. This is shown in figure 5.14. The higher amplitude of the kinking, and stronger deviation from axisymmetry has caused the region around the two magnetic axes to become chaotic.

Even when the field is chaotic, the poloidal field still decays faster than the toroidal, and the total magnetic field strength becomes lower. Eventually the magnetic field decays enough that the structure is no longer susceptible to the nonaxisymmetric perturbation, and the magnetic field organizes again to a configuration consisting of nested toroidal magnetic surfaces.

The nonaxisymmetric perturbations that result in the formation of secondary islands and the appearance of chaotic regions in the magnetic field puts limits on the regime in which the self-organizing processes operate to form the toroidal structure. An important parameter to quantify this is the plasma β the ratio of hydrostatic pressure to magnetic pressure: $\beta = \frac{p}{B^2/2}$. We define the plasma β in our structures by taking for the magnetic pressure the maximum of B^2 and for the pressure the external pressure of $p = 1$. At lower β the magnetic forces become more significant, and the dip in the pressure becomes larger. This results in a net larger influx of plasma fluid through Pfirsch-Schlüter diffusion, which leads to stronger kinking of the magnetic axis. The configurations that do not show any island formation have a $\beta \gg 1$, for example the configuration with $\eta = 2 \times 10^{-4}$ and $B_0 = 0.05$ has a maximum field strength at $t_\eta = 0.01$ of $B^2_{\max} = 0.06$. This gives a plasma β of 33.3. Even the fields that demonstrate significant magnetic chaos have a $\beta \geq 1$. The chaotic magnetic configuration shown in figure 5.14 has a maximum magnetic field strength at $t = 0.01 t_\eta$ of $B^2_{\max} = 0.16$ giving a plasma $\beta = 12.5$. It is important to note that the onset of the nonaxisymmetric configuration and resultant magnetic chaos are more prevalent at higher values of ι_0, as the field with $\iota_0 = 3$ and $B_0 = 0.2$ shown in figure 5.5 does not kink. Though the configurations considered here are chaotic at high values of β, it is possible that axisymmetric self-organized equilibria with $\iota_0 \leq 1$ remain ordered at much lower plasma β. This is an interesting path of investigation for future studies.

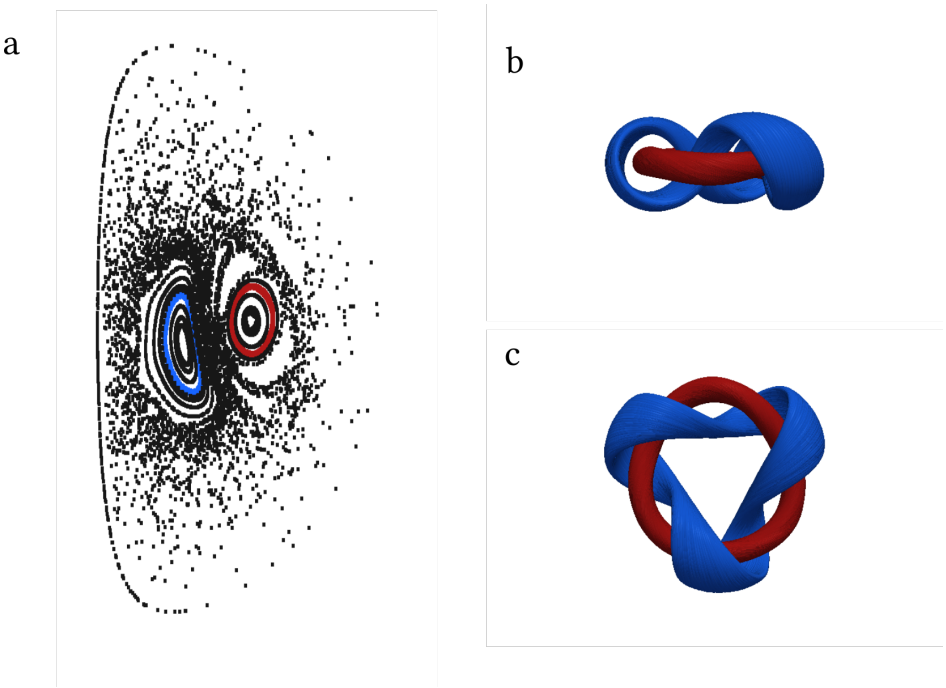

Figure 5.14: Magnetic structure showing the creation of a chaotic region at higher magnetic field strengths. $B_0 = 0.20$, $\eta = 2 \times 10^{-4}$ taken at time $t_\eta = 0.023$. (a) Poincaré plot. Two magnetic islands are seen in the chaotic region. (b) Side view of the magnetic surfaces. (c) Top view of the magnetic surfaces.

5.8 Conclusions and discussion

In this chapter we have shown many of the interesting phenomena that occur when a self-organizing helical magnetic structure decays on a resistive timescale. We have observed how the rotational transform profile becomes nearly flat with a slight negative curvature such that the rotational transform is highest on the magnetic axis. As the resistivity decreases the magnetic field strength, the poloidal field decreases faster than the toroidal field, such that the rotational transform decreases according to a power law. The slope of this decrease depends on the aspect ratio of the structure, which is higher for fields with a higher initial rotational transform.

Due to Pfirsch-Schlüter diffusion there is a net inflow of plasma onto the magnetic axis leading to an increase in the major radius of the magnetic structure. We have also

observed that when the magnetic field strength is higher and the resistivity is lower, this net influx onto the central magnetic surfaces results in a higher pressure than an axisymmetric equilibrium can maintain, and the magnetic axis becomes kinked. This introduces nonaxisymmetric flux into the configuration, which results in magnetic islands at resonant magnetic surfaces. At low field strength this leads to a core interchange mechanism such that the magnetic axis is replaced by the island. Due to the resistivity predominantly acting on field components with larger spatial gradients, the nonaxisymmetric components decay faster, and the fields eventually return to axisymmetry.

Important for the motion of the islands is the rotational transform profile. Initially this rotational transform profile starts out with positive curvature, but soon after it becomes nearly flat, with a slight negative curvature. The rotational transform is continuously lowering in the entire structure, whilst the profile remains roughly self-similar in shape. In the presence of nonaxisymmetric perturbations resonant surfaces will be broken up into island chains. Due to the slight negative curvature in the rotational transform profile these resonant surfaces move inwards towards the magnetic axis. The motion of the magnetic islands can thus be seen as an effect of continuously lowering rotational transform in the structure, which causes the resonant magnetic surfaces to continually move inward toward the magnetic axis.

The lowering of the rotational transform profile is a robust finding in these simulations which indicates that the poloidal magnetic field decays at a faster rate than the toroidal magnetic field. It is important to note that this result is only robust in our simplified isothermal MHD model, with a spatially constant resistivity. In reactor plasmas the plasma temperature is lower near the reactor wall, and hence the resistivity of the plasma is higher. The poloidal magnetic field is generated by the plasma currents passing through this region. In such a configuration it is observed that the toroidal magnetic field decays faster, and the rotational transform increases in time [126]. The self-organized structure however is a localized magnetic excitation embedded in a high-pressure plasma, and in for example the case of magnetic clouds, it is generally observed that the temperature is lowered within the cloud [78].

There is much still to be learned from the self-organizing processes acting on localized magnetic excitations in a plasma. In this chapter we have shown many of the phenomena that can occur in these fields on resistive timescales. To our knowledge these processes have never been investigated in this specific context: A localized magnetic field with helicity relaxing against a finite external pressure. This is however a situation that can occur on any size scale, from radio bubbles emitted from galaxies to magnetic clouds and all the way down to meter or millimeter scale experiments in the laboratory. The situation we have studied is notably different from the configurations generally found in fusion experiments, that have a well-defined boundary and external coils that generate a large portion of the magnetic fields. Nevertheless, these fields exhibit island

formation, nonaxisymmetric perturbations, onset of magnetic chaos, self-organization into equilibrium configurations and many more phenomena that are often observed and are a matter of current investigation in magnetic confinement research. Not only can the results from magnetic confinement research be used to understand the phenomena presented here, the self-organized equilibria also offer an elegant and simple configuration in which these processes can be studied.

Acknowledgments

This chapter was brought about with help from H. De Blank, T. A. de Jong, D. Kok and D. Bouwmeester. We would like to thank Joost Opschoor for his work on KAM theory and magnetic islands.